2019

The fate and prognostic implications of hyperreflective crystalline deposits in nonneovascular age-related macular degeneration

S. Fragiotta

P. Fernáandez-Avellaneda

M. P. Breazzano

C. A. Curcio

B. C. Leong

See next page for additional authors

Authors

S. Fragiotta, P. Fernáandez-Avellaneda, M. P. Breazzano, C. A. Curcio, B. C. Leong, K. Kato, L. A. Yannuzzi, and K. B. Freund

The Fate and Prognostic Implications of Hyperreflective Crystalline Deposits in Nonneovascular Age-Related Macular Degeneration

Serena Fragiotta,[1–3] Pedro Fernández-Avellaneda,[1,2,4] Mark P. Breazzano,[1,2,5,6] Christine A. Curcio,[7] Belinda C. S. Leong,[1,2] Kenneth Kato,[1] Lawrence A. Yannuzzi,[1,2,5,6] and K. Bailey Freund[1,2,5,6]

[1]Vitreous Retina Macula Consultants of New York, New York, New York, United States
[2]LuEsther T. Mertz Retinal Research Center, Manhattan Eye, Ear and Throat Hospital, New York, New York, United States
[3]Department of Medico-Surgical Sciences and Biotechnologies, U.O.S.D. Ophthalmology, Sapienza University of Rome, Rome, Italy
[4]Department of Ophthalmology, Basurto University Hospital, Bilbao, Spain
[5]Department of Ophthalmology, New York University School of Medicine, New York, New York, United States
[6]Columbia University College of Physicians and Surgeons, Harkness Eye Institute, New York, New York, United States
[7]Department of Ophthalmology and Visual Science, University of Alabama at Birmingham, School of Medicine, Birmingham, Alabama, United States

Correspondence: K. Bailey Freund, Vitreous Retina Macula Consultants of New York, 950 Third Avenue, New York, NY 10022, USA; kbfnyf@aol.com.

Submitted: January 7, 2019
Accepted: May 11, 2019

Citation: Fragiotta S, Fernández-Avellaneda P, Breazzano MP, et al. The fate and prognostic implications of hyperreflective crystalline deposits in nonneovascular age-related macular degeneration. *Invest Ophthalmol Vis Sci*. 2019;60:3100–3109. https://doi.org/10.1167/iovs.19-26589

Purpose. To explore patterns of disease progression in nonneovascular age-related macular degeneration (AMD) associated with hyperreflective crystalline deposits (HCDs) in the subretinal pigment epithelium–basal laminar space.

Methods. Retrospective review of medical records, multimodal imaging, and longitudinal eye-tracked near-infrared reflectance (NIR) and optical coherence tomography (OCT) spanning ≥2 years. NIR/OCT images were analyzed with ImageJ software to identify HCD morphology and location. Associated macular complications were reviewed from the time of HCD detection to the most recent follow-up, using NIR/OCT.

Results. Thirty-three eyes with HCDs from 33 patients (mean age: 72 ± 7.5 years) had 46.7 months (95% confidence limits: 33.7, 59.6) of serial eye-tracked NIR/OCT follow-up. Baseline best-corrected visual acuity (BCVA) was 0.44 logMAR (Snellen equivalent 20/55). At a mean of 11.3 months (3.1, 19.6) after HCD detection, 31/33 (93.9%) eyes had developed macular complications including de novo areas of complete retinal pigment epithelium and outer retinal atrophy (cRORA) in 21/33 (64%) eyes, enlargement of preexisting cRORA in 4/33 (12%) eyes, and incident macular neovascularization in 3/33 (9%) eyes. Movement and clearance of HCDs in 9/33 (27%) eyes was associated with enlargement of preexisting cRORA ($r = 0.44$, $P = 0.02$). BCVA at the last follow-up visit had decreased to 0.72 logMAR (20/105).

Conclusions. Eyes with nonneovascular AMD demonstrating HCDs are at risk for vision loss due to macular complications, particularly when movement and clearance of these structures appear on multimodal imaging. HCD reflectivity and dynamism may be amenable to automated recognition and analysis to assess cellular activity related to drusen end-stages.

Keywords: cholesterol, crystals, age-related macular degeneration, hyperreflective crystalline deposits, spectral-domain optical coherence tomography, macular neovascularization, complete retinal pigment epithelium and outer retinal atrophy, drusen, refractile deposits

Age-related macular degeneration (AMD) is a leading cause of central vision loss in older persons worldwide due to the loss of photoreceptors, retinal pigment epithelium (RPE), and choriocapillaris endothelium in the context of characteristic extracellular deposits between visual cells and the circulation.[1] Neovascular AMD is managed with anti–vascular endothelial growth factor therapy, and some patients with intermediate AMD benefit from dietary supplementation of antioxidants.[2,3] With recent trial failures of agents targeting geographic atrophy (GA), new approaches are needed for earlier AMD stages. This goal can be served by elucidating the timeline and microarchitecture of atrophy via histologically validated, multimodal clinical imaging, anchored by eye-tracked optical coherence tomography (OCT). Close examination of advanced disease, followed by backtracking to precursors, can provide new mechanistic insights.[4–7] An international working group is currently documenting indicators of progression to atrophy.[8]

Fleckenstein et al.[9] were the first to describe highly reflective lines at the fourth reflective band on OCT, that is, at the level of the RPE/Bruch's membrane (BrM) complex in eyes with nonneovascular AMD.[10] These lines, observed in perilesional zones of GA, correspond to lesions with mirror-like reflectivity on near-infrared reflectance (NIR). The authors have termed these lines "segmented plaques," and propose that they represent BrM "densification," referring to published histology.[11,12] Detected in 44% of patients with GA, these lines have

been associated with the development of multifocal patches of macular atrophy.[13] Querques et al.[14] have found similar highly reflective lines on OCT that are obliquely oriented (i.e., separate from and floating above BrM) within regressing drusen. These authors hypothesize that coiled, membranous debris (soft druse material) accumulating between RPE and BrM may calcify during drusen progression, further postulating a split and inward bowing of BrM to account for the position and orientation of the lines. Others have illustrated similar highly reflective lines on OCT and also attributed them to calcification of drusen.[15]

Distinctive multilayered lines corresponding to mirror-like reflective plaques in clinical NIR imaging have been found within vascularized pigment epithelial detachments in neovascular AMD and called by one of us (KBF) the "onion sign."[16–18] Demonstration that the onion sign could represent cholesterol crystals has come from subsequent histopathology,[16] in which solvents used for tissue processing dissolve the crystals and create a space in the tissue known as "cholesterol clefts," a process well known from cardiovascular histopathology. To form the clinically recognizable onion sign, an aqueous environment in the sub-RPE–basal laminar (BL) space is hypothesized to permit supersaturation and precipitation of cholesterol derived from dying cells, plasma exudate, or both.[16] Cholesterol crystals confirmed by polarizing microscopy of fluid aspirates also form in Coats disease[19] and in this disorder, highly reflective linear structures on OCT B-scans correlate with needle-like clefts on histology.[20,21] Crystallization can also occur in environments with less fluid. Cholesterol clefts reported within fibrovascular scars of neovascular AMD in 1977[11] were directly correlated to highly reflective lines in clinical OCT in 2018.[22] Recently, our group published a clinicopathologic correlation of an eye with GA secondary to nonneovascular AMD,[23] which manifested highly reflective lines on OCT like those described by Fleckenstein et al.[9] and Querques et al.[14] We identified, as the source of hyperreflectivity, cholesterol clefts within avascular fibrosis, a material that can replace drusen contents.[12] Since the molecular composition of crystals was not directly assayed in these studies, we have chosen to describe their OCT signatures in this report, calling them "hyperreflective crystalline deposits" (HCDs).

Little is known about specific clinical AMD phenotypes leading to HCDs in nonneovascular AMD, the fate of HCDs once present, and the natural course of eyes demonstrating these lesions. We sought to answer these questions through a retrospective review of multimodal imaging, including longitudinal eye-tracked NIR/OCT, in eyes showing HCDs associated with nonneovascular AMD at some point during their follow-up. Herein, we explored prognostic implications of HCD, their association with other AMD-related fundus findings, and their evolution over an extended follow-up. In a related manuscript in preparation, we will define precursor lesions leading to the appearance of HCDs.

Methods

This was a retrospective review of medical records and retinal imaging from patients with nonneovascular AMD associated with HCDs at some time during their follow-up who were examined between November 2008 and February 2018. Each patient had been examined by one of two retinal specialists (KBF, LAY) at Vitreous Retina Macula Consultants of New York, a large tertiary referral practice for retinal diseases.

This study adhered to the tenets of the Declaration of Helsinki and complied with the Health Insurance Portability and Accountability Act of 1996. It was approved by the Institutional Review Board (IRB) committee at the Western IRB.

Inclusion criteria were presence of highly reflective subretinal or sub-RPE lines on OCT B-scans colocalized to irregular highly reflective mirror-like lesions on NIR; ≥2-year follow-up with serial, eye-tracked OCT B-scans; and complete medical records.

Exclusion criteria included an interruption in the sequence of tracked OCT B-scans before the 2-year follow-up, media opacities preventing high-quality OCT, vitreomacular interface disorders (i.e., vitreomacular traction or macular pucker), evidence of retinal vascular disease or other retinal disease associated with retinal edema and/or lipid deposition, or the presence of macular neovascularization (MNV) or RPE tear at baseline.

Medical history concerning cardiovascular events and risk factors was reviewed because use of lipid-lowering medications has previously been reported, by Pang et al.,[16] to be associated with HCDs in neovascular AMD.

Clinical Staging

HCDs were defined on OCT as highly reflective lines located anteriorly to BrM and posteriorly to any remaining RPE attached to either its native basal lamina or basal laminar deposit (BLamD), that is, in the sub-RPE–BL space.[14,16,24] The HCDs had either a single linear or multilaminar appearance on OCT B-scans with a corresponding hyperreflective plaque on NIR. On clinical ophthalmoscopic examination, the HCDs appeared as brilliant yellow lesions, typically within areas of hypopigmentation and distinct from accompanying drusen (Fig. 1). Some eyes had HCDs at multiple locations. In some eyes, HCDs occurred in clusters (Figs. 1D, 1E).

In patients with bilateral HCDs, one eye was randomly selected as the study eye. OCT B-scan data and related multimodal imaging were reviewed independently by two graders (SF, PF-A). In case of disagreement, a senior retinal specialist (KBF) was consulted to resolve the discrepancies between graders by open adjudication.

Refractile Drusen and Macular Complications

Refractile drusen or "calcified drusen" were identified as chalky-white, shiny or glistening in appearance on ophthalmoscopy[25–27] and can appear similar to HCDs on color photography. However, refractile drusen show heterogeneous internal reflectivity (HIRD) and a hyporeflective core, now attributed to "calcific nodules,"[28] in contrast to the linear shape of HCDs (Fig. 2).

Drusenoid pigment epithelial detachment (PED) was defined according to Age-Related Eye Disease Study as a pale yellow or white large mound measuring at least 350 μm in the narrowest diameter with an elevated appearance on stereoscopic color fundus photographs.[29] Drusenoid PEDs are distinguishable from serous and hemorrhagic PEDs by clinical features revealed on ophthalmoscopic examination and fluorescein angiography (FA).[30]

MNV was defined as new vessel growth detected with FA and/or OCT angiography.

Complete RPE and outer retinal atrophy (cRORA) met diagnostic criteria of the Classification of Atrophy (CAM) Report 3[8] as follows: (1) a region of hypertransmission at least 250 μm in diameter; (2) attenuation and/or disruption of the RPE at least 250 μm in diameter; and (3) loss of overlying interdigitation zone, ellipsoid zone (EZ), and external limiting membrane (ELM)[10] as well as thinning of the outer nuclear layer. Incomplete RPE and outer retinal atrophy (iRORA) was defined as irregular or interrupted EZ, ELM, and RPE band with

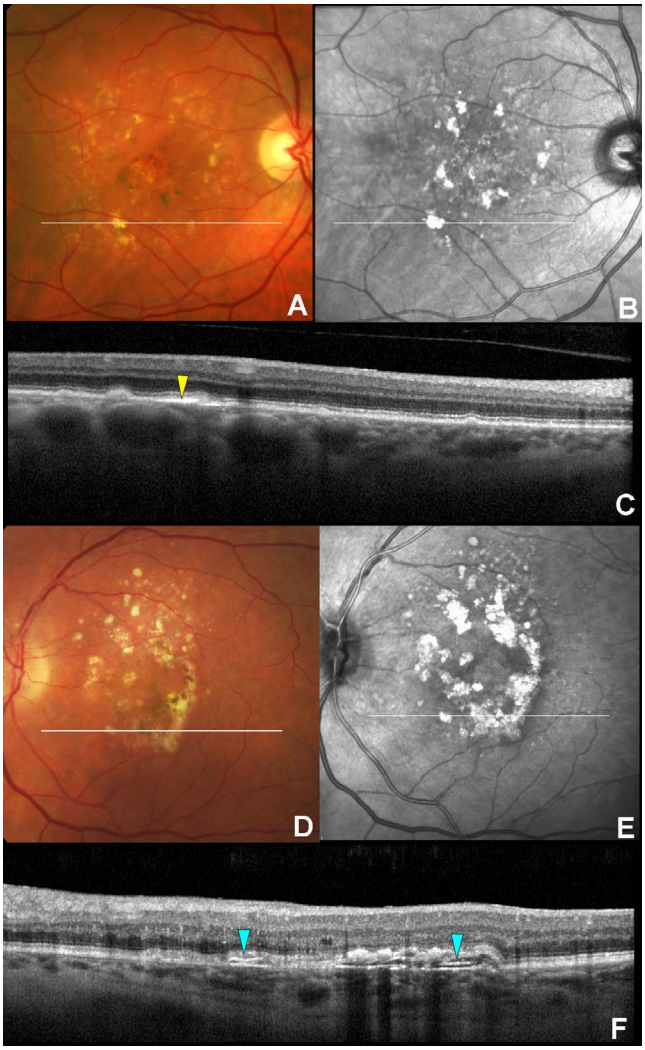

FIGURE 1. Multimodal imaging of HCDs. A representative case of 67-year-old male with nonneovascular AMD and multiple HCDs in the right eye: (**A**) Color photograph of the right eye shows scattered bright yellow lesions in the macula. (**B**) NIR shows focal areas of high mirror-like reflectivity. (**C**) Optical coherence tomography B-scan through a hyperreflective HCD in the inferior macula (*white line* on **A**, **B**) demonstrates a highly reflective linear structure (*yellow arrowhead*) located between RPE with underlying BLamD and Bruch's membrane. A 71-year-old female with nonneovascular AMD and multiple aggregated HCDs in the left eye: (**D**) Color photograph of the left eye shows multiple brilliant yellow deposits encircling the fovea. (**E**) NIR shows the corresponding HCDs as highly reflective lesions. (**F**) An OCT B-scan through an area of aggregated HCDs (*white line* on **D**, **E**) shows multiple linear hyperreflective deposits located within a split RPE/Bruch's membrane complex (i.e., in the sub-RPE–BL space, where BL means either basal lamina or basal laminar deposits) (*light blue arrowheads*).

nonhomogeneous hypertransmission.[8] The border of cRORA was determined by both the presence of choroidal hypertransmission and descent of the ELM toward BrM on each cross-sectional scan considered, as described.[31]

The Early Treatment Diabetic Retinopathy Study (ETDRS) grid was displayed and centered on the NIR image by using an SD-OCT cross-sectional scan to reference the foveal center. cRORA within the central 1-mm diameter subfield of the ETDRS grid was graded as involving the foveal center in any case. The fovea was graded as spared in presence of foveal depression with preserved inner and outer retinal layers.[32] In case of foveal sparing, if the greater extension of cRORA was located between central subfield and the 3-mm (outer) diameter ring it was graded as parafoveal; and between 3-mm and the 6-mm (outer) diameter ring, as perifoveal.

Multimodal Imaging

SD-OCT was performed with Spectralis HRA+OCT (acquisition software version 6.8.1.0; Heidelberg Engineering, Heidelberg, Germany;).

When available, the OCT scan pattern used for analysis was 30° × 20° (8.8 mm × 5.7 mm) centered on the fovea and composed of 49 B-scans with a nominal interscan distance of 121 μm. The minimum acceptable scan pattern was 20° × 15° (5.8 × 4.3 mm) centered on the fovea with a maximum nominal interscan distance of 224 μm. To minimize speckle noise and enhance visualization of ELM descent,[31] automatic real-time tracking (ART) mode was typically set between 10 to 20 frames and Scan Quality Factor ≥ 25 decibels. NIR was acquired simultaneously with SD-OCT B-scans by using an excitation wavelength of 870 nm.[33]

Color photographs, fundus autofluorescence, and red-free images were obtained by using Topcon TRC-50DX fundus camera (Topcon Medical Systems, Paramus, NJ, USA). Fundus autofluorescence images were obtained by using an excitation filter of 535 to 580 nm and a barrier filter of 675 to 715 nm. Red-free digital monochromatic photographs were obtained by using the standard green filter of the fundus camera.[34]

Characterization of HCD Movement

To estimate a rate of HCD movement in the sub-RPE–BL space, individual HCDs were followed and their positions recorded in a foveocentric coordinate system. NIR images from the SD-OCT device were extrapolated by using the "extract fundus image" function and then exported as a tagged image file (TIF) format. Serial NIR images were aligned (Photoshop Creative Cloud, version 20.0.1; Adobe Inc., San Jose, CA, USA) as follows: Go to File > Scripts > Load Files into Stack, select all layers, and Edit > Auto-Align Layers. Aligned images were saved (File > Scripts > Export Layers to Files) for analysis with the open source imaging processing software FIJI (software version 2.0.0-rc-68/1.52e; http://fiji.sc).[35]

Spatial calibration of serial NIR images on ImageJ (Analyze > Set Scale) was obtained by using the factor scale provided by Heidelberg software for each case (Image > Info). However, since individual variations in corneal curvature were not entered in the Eye Data field during acquisition mode, the default axial length (and thus default ocular magnification) was automatically calculated by the software. To bypass inaccuracies in lateral scaling factor (μm/pixel in *x*- and *y*-direction) distance measurements were reported as degrees. Before tracking HCDs, the foveal center was identified by using anatomic hallmarks in cross-sectional SD-OCT: foveal depression, centripetal displacement of inner retinal layers and outer plexiform layer, outer nuclear layer thickening, and inward rise of the ELM and EZ. Once the foveal center was identified and labeled, the cursor was moved over the center by using ImageJ (http://imagej.nih.gov/ij/; provided in the public domain by the National Institutes of Health, Bethesda, MD, USA), and the coordinates displayed on the status bar were input and set with "Origin (Pixels)" (Image>Properties>Origin (Pixels)).

HCDs were manually selected by using the polygonal selection tool at each follow-up time point, and coordinates were obtained by using Analyze>Measure function in FIJI. In cases of multiple HCDs, each single HCD was independently tracked (e.g., Track1, Track2).

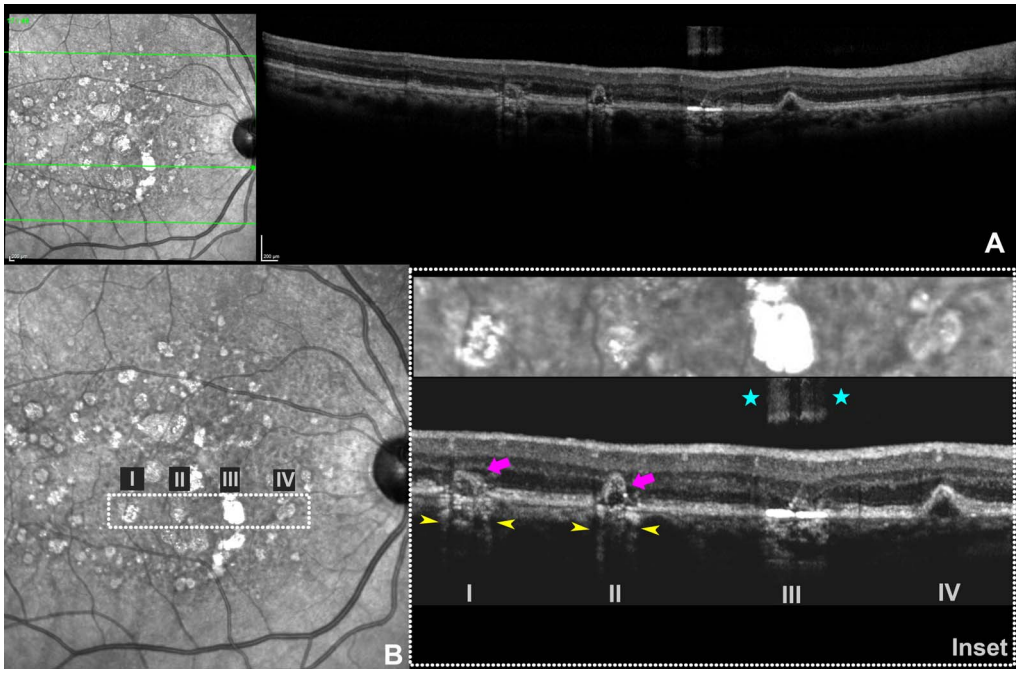

FIGURE 2. Distinguishing NIR and OCT findings of HCDs and refractile drusen. (**A**) NIR and OCT B-scan through several refractile drusen and HCDs. (**B**) Extracted NIR with dotted inset showing the characteristic speckled reflectivity of three refractile drusen (I, II, and IV) and the more intense mirror-like reflectivity of HCDs (III). The OCT B-scan (*lower right*) corresponds to the area within the inset. The OCT appearance of refractile drusen has been termed "heterogeneous internal reflectivity of drusen" and consists of a cap containing hyperreflective spherules (*purple arrows*) and a hyporeflective core representing a calcific nodule. Hypertransmission (*yellow arrowheads*) is evident at the border of the refractile drusen. The OCT appearance of HCDs is a highly reflective linear structure anterior to Bruch's membrane. The high reflectivity of HCDs can produce imaging artifacts (*light blue stars*) due to the OCT detector becoming saturated (unpublished data).

Statistical Analysis

LogMAR best-corrected visual acuity (BCVA) was calculated by the procedure of Holladay[36] and reported along with Snellen equivalent. Distribution normality was verified through Shapiro-Wilk normality test. Spearman's rank correlation coefficient or Kendall's tau coefficient was calculated to determine the existence of a monotonic relationship as well as the strength and direction between two variables on a scale that is at least ordinal. Multivariate analysis of variance for repeated measures was calculated for BCVA obtained at different time points. Means are reported with 95% confidence limits for nonnormal distribution. P values less than 0.05 were each considered statistically significant. All calculations were performed by using Statistical Package for the Social Sciences (SPSS) software (ver. 20; SPSS, Inc., Chicago, IL, USA).

RESULTS

A total of 76 eyes of 54 patients with AMD and HCDs were initially identified, of which 28 eyes of 21 patients were excluded owing to the presence of MNV at baseline (23/28, 82.14%), insufficient eye-tracked OCT follow-up (4/28, 14.3%), or concurrent macular pucker (1/28, 3.6%). In 15 patients with two eligible eyes, one eye was excluded at random. Demographic characteristics for 33 study eyes of 33 patients are reported in Table 1. Regarding the use of statins, our population exhibited a rate (13/33 patients, 39.4%) similar to that of the general population in the United States (range, 39.1%–54.4%) but significantly lower than the cohort exhibiting an onion sign in neovascular AMD (11/15, 73%; $P < 0.03$), as previously reported.[16,37]

Baseline Clinical Features

Baseline BCVA was 0.44 (95% confidence interval [CI]: 0.3, 0.6) logMAR (20/55 Snellen equivalent). By OCT, HCDs appeared between the RPE and BrM in all cases (Figs. 1C–F). In 31/33 (93.93%) eyes, HCDs were parallel to and not resolvable from BrM, and in 1/33 (3%) HCDs were parallel to and resolvable from BrM. In 1/33 (3%) eyes, HCDs were obliquely oriented with respect to the underlying BrM. In 26/33 (78.8%) cases, multiple HCDs were detected within the same eye. Clusters of HCDs were present in 24/33 (73%) eyes. On NIR, HCDs, either single or in clusters, appeared as hyperreflective roundish spots in all eyes (33/33, 100%). Multilaminar HCDs were detected on OCT in 17/33 (51.5%) eyes (Fig. 1). Refractile drusen were found in 11/33 (33.33%) eyes.

Longitudinal Analysis

The mean follow-up time with serial eye-tracked NIR/OCT was 46.7 months (95% CI: 33.7, 59.6). At the time of the most recent NIR/OCT evaluation, HCDs were still detected in 23/33 (69.7%) eyes. BCVA had declined to 0.72 (95% CI: 0.5, 0.9) logMAR (20/105), with a mean difference of 0.27 logMAR between the first and final visits ($P < 0.001$).

The BCVA decline over time ($F_{2,31} = 9.8$, $P < 0.001$) was significant between different time points considered in post hoc analysis, particularly with the disappearance of previously apparent HCDs ($P = 0.02$) and between HCD appearance and last visit ($P < 0.001$). Table 2 summarizes BCVA changes for each follow-up time considered.

The presence of multiple HCDs organized in clusters on NIR was also related with decreasing BCVA recorded at the time of HCD appearance ($r = -0.51$, $P = 0.002$), HCD

Table 1. Main Characteristics of the Study Group at Baseline

	Subjects (n = 33 Eyes)
Age, mean (SD), y	71.83 (7.49)
Sex, female, n (%)	25 (75.8)
Visual acuity, mean (SD), logMAR	0.32 (0.3)
Bilateral, n (%)	15 (45.4)
Systemic factors, n (%)	
Hypercholesterolemia	16 (48.5)
Statin use	13 (39.4)
Hypertension	17 (51.5)
Cardiovascular disease	4 (12.1)
Fellow eye status, n (%)	
MNV	14 (42.4)
PED	10 (30.3)
cRORA	4 (12.1)
NNV-AMD	4 (12.1)
Phthisis bulbi	1 (3)

logMAR, logarithm of the minimum angle of resolution; NNV-AMD, nonneovascular age-related macular degeneration, excluding late stages; SD, standard deviation.

disappearance (r = –0.47, P = 0.006), and last follow-up available (r = –0.47, P < 0.001).

Thirty-one patients (93.9%) developed macular complications after a mean of 11.3 months (95% CI: 3.1, 19.6) from the first tracked OCT evaluation. The most common macular complication was incident cRORA in 21/33 (63.6%) eyes, followed by enlargement of existing cRORA in 4/33 (12.1%) eyes, MNV in 3/33 (9.1%) eyes, RPE aperture[39] in 2/33 (6.1%) eyes, and lamellar macular hole in 1/33 (3%) eyes. cRORA involved the foveal center within the central 1-mm-diameter subfield of the ETDRS grid in 18/25 (72%) eyes, in the parafovea of 6/25 (24%) eyes, and the perifovea in only 1/25 (4%) eyes.

The mean duration of HCD visibility was 39.21 months (95% CI: 27.3, 51.13). This period was significantly higher among patients who developed MNV (79.4 ± 16.5 months, P = 0.001).

Hyperreflective Crystalline Deposit Turnover and Movement

HCDs exhibited a certain degree of remodeling associated with cRORA expansion, resulting in movement, clearance, or both, during follow-up. In 9/33 (27.3%) eyes, new HCDs appeared, with subsequent fragmentation and resorption in some cases. In 15/33 (45.4%) eyes, small collections of adjacent HCDs coalesced into larger aggregations which then showed partial or complete clearance (Fig. 3). In the remaining 7/33 (21%) eyes, clearance occurred without prior coalescence (Fig. 4). In only 2/33 (6%) eyes, the HCD morphology remain unchanged over the course of follow-up.

Movement of HCDs was detected in 9/33 (27.3%) cases. The presence of movement was associated with a progressive cRORA enlargement over tracked follow-up time (r = 0.44, P = 0.02) and inversely related to the presence of HCDs at last follow-up (r = –0.63, P < 0.001; see also Fig. 5 and Supplementary Video S1).

A total of 97 tracking points were analyzed in nine patients demonstrating HCD movement over time. Table 3 shows the main features of HCD movement characteristics in this patient subgroup. The total area occupied by HCDs was directly related to the distance from the foveal center (r = 0.49, P < 0.001). The rate of movement was 0.68 deg/mo (95% CI: –6.98, 5.62). All nine tracked eyes developed macular complications during the period of HCD movement and clearance (Table 4). De novo cRORA proceeded from iRORA in all cases (100%).

Table 2. Visual Loss in Patients With Hyperreflective Crystalline Deposits During Follow-up

Stage	Visual Acuity		Years From Baseline, Mean (SD)
	LogMAR	Snellen Equivalent	
First HCD appearance	0.44 ± 0.21	20/55	–
HCD disappearance	0.64 ± 0.55	20/87	3.26 (2.8)
Last FU	0.72 ± 0.56	20/150	3.92 (3.1)

FU, follow-up.

At the follow-up preceding HCD movement, all tracked eyes presented multiple HCDs (9/9, 100%) scattered around the central fovea in 5/9 (55.5%) cases, at the border of atrophy in 3/9 (33.33%) cases, and involving the foveal center in only 1 (11.1%) case. During movement, they tended to scatter at the border of atrophy in 7/9 (77.8%) cases, whereas, in the remaining 2 (22.2%) cases, they were distributed within the central fovea (1-mm-diameter ETDRS central subfield). HCDs were no longer visible in 7/9 (77.8%) cases at the end of tracking.

Movement coordinates of seven eyes that developed cRORA were recorded in 47 different tracking points and correlated with cRORA area measurements at each single point. Faster-growing cRORA was related to HCD proximity to the fovea (r = –0.36, P = 0.02).

At the most recent eye-tracked OCT examination, HCDs were located at the boundary of cRORA in 12/33 (36.4%) eyes, within the area of cRORA in 12/33 (36.4%) eyes, both locations in 3/33 (9.1%) eyes, at the edge of collapsed PED in 3/33 (9.1%) eyes without retinal atrophy, at the border of an area of drusen resolution in 1/33 (3%) eyes, within an RPE aperture[38] in 1/33 (3%) eyes, and scattered around the area of retinal atrophy in 1/33 (3%) cases.

Discussion

The present study investigated the fate and prognostic implications of HCDs in eyes with nonneovascular AMD. We demonstrated that HCDs are dynamic in nature with evidence for de novo production, fragmentation, conglomeration, and resorption. Eyes with HCDs developed macular complications in almost all cases (93.4%) after a mean longitudinal follow-up

Table 3. Main Features in Hyperreflective Crystalline Deposit Migration Subgroup

	Subjects (n = 9 Eyes)
Age, mean (SD), y	72.4 (7.9)
Sex, female, n (%)	7 (77.8)
Visual acuity, mean (SD), logMAR	0.3 (0.1)
Bilateral, n (%)	5 (55.6)
Baseline distance from fovea, °	47.4 (28.5)
Final distance from fovea, °	31.9 (29.3)
Distance from previous location, °	18.4 (28.5)
Rate of movement, °/mo	0.68 (3.16)
Area of HCDs, global, μm	417.6 (128.6)

Euclidian distances were calculated for x and y coordinates; the movement was calculated by using fovea coordinates for each single case examined.

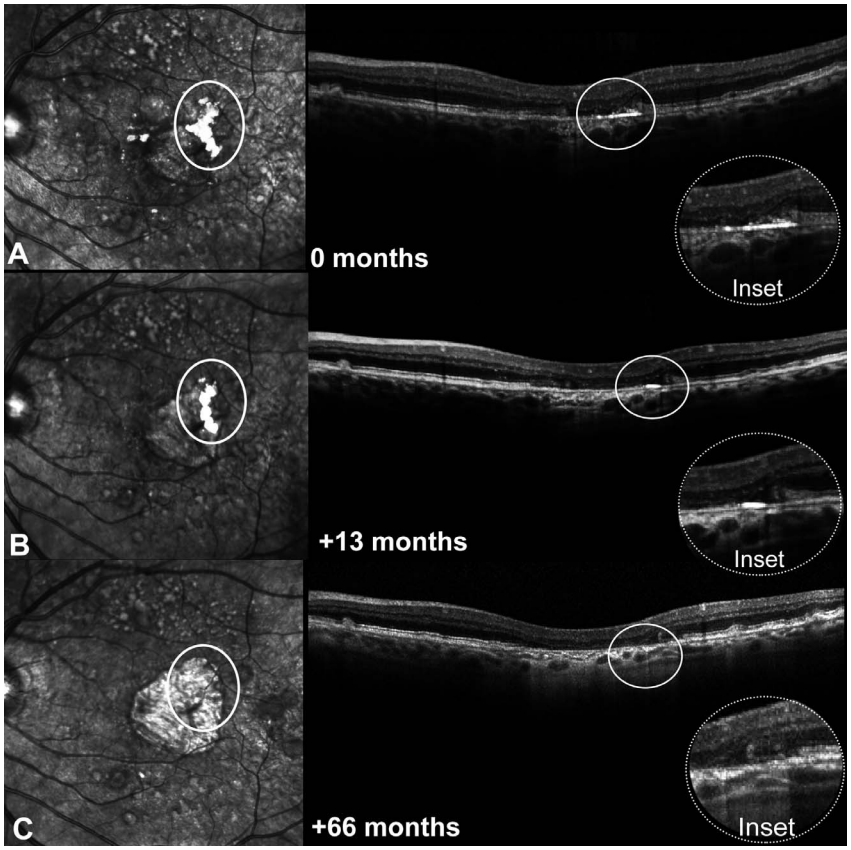

FIGURE 3. Dynamism of highly reflective HCDs in nonneovascular age-related macular degeneration. Serial tracked NIR and SD-OCT of a 54-year-old man showing HCDs (*white circle*) in his left eye. (**A**) Crystals are aggregated at the edge of outer retinal layers and RPE atrophy with overlying subsidence of the outer plexiform layer. (**B**) There is both consolidation and fragmentation of crystals at the margins, which are partially covered by RPE with either its native basal lamina or basal laminar deposit (RPE-BL). (**C**) Complete resorption without movement.

of 11.3 months from the first-tracked OCT. The most common complication was new cRORA (63.6%) or enlargement of established cRORA (12.1%) followed by MNV (9.1%). cRORA tends to involve the foveal region (72%) over the parafoveal location (24%). BCVA declined over time during HCD turnover, markedly deteriorating in relation to the interval between HCD appearance and disappearance. Coalescence of HCDs in clusters represented a further negative prognostic factor for visual acuity. Additionally, in some cases, HCDs moved along BM around the fovea, which was an important predictor for subsequent cRORA, as demonstrated by progressive enlargement of cRORA in relation to distance covered by HCDs. As previously reported, eyes with hyperreflective foci (odds ratio: 11.21) drusenoid lesions with heterogeneous internal reflectivity (odds ratio: 7) and refractile drusen (odds ratio: 6.36 to late AMD) also have an increased risk of progression into new atrophy onset.[27,28,39] Although our study design did not allow calculation of odds ratio, the incidence of new cRORA (63.3% of eyes) was similar to the incidence reported for eyes with refractile drusen (59.1%).[27]

TABLE 4. Macular Complications During Movement of Hyperreflective Crystalline Deposits

Macular Complications, *N* (%)	Subjects (n = 9 Eyes)
De novo cRORA	4 (44.4)
Enlargement of cRORA	3 (33.3)
MNV	1 (11.1)
RPE aperture	1 (11.1)

Our data add to growing literature that establishes the identity of reflective features signifying progression to advanced AMD. The distinctive OCT appearance of cholesterol crystals as hyperreflective linear deposits without shadowing due to their high transparency has been confirmed by direct clinicopathologic correlations between SD-OCT images and histopathology in several disorders resulting from chronic exudation.[16,17,21,22] This pathogenic mechanism causing cholesterol clefts seen histologically validated the typical stratified hyperreflective lines visible on OCT, the so-called onion sign.[16,17] Despite the undeniable role of chronic exudation, recent clinicopathologic correlations have identified cholesterol clefts corresponding to hyperreflective plaques on NIR and single hyperreflective lines lying on BrM on cross-sectional B-scan in nonneovascular AMD.[23]

Mirror-like hyperreflective lines that appear in or near BrM, representing sparse cholesterol crystals within the fluid or fibrotic material that replaces oily drusen, have been recently differentiated from calcified structures in drusen.[28,22,40] Refractile drusen were first described by Suzuki et al.[26] as mound-like elevations containing multiple hyperreflective dots now known from histopathology and microanalysis to originate from small highly crystalline whitlockite spherules.[28] OCT reflectivity signatures of calcified structures associated with cRORA development include reflective dots (spherules) and HIRD with hyporeflective core and hyperreflective cap (nodules).[28] Calcified plaques within BrM of older eyes have been long recognized but do not yet have a defined reflectivity

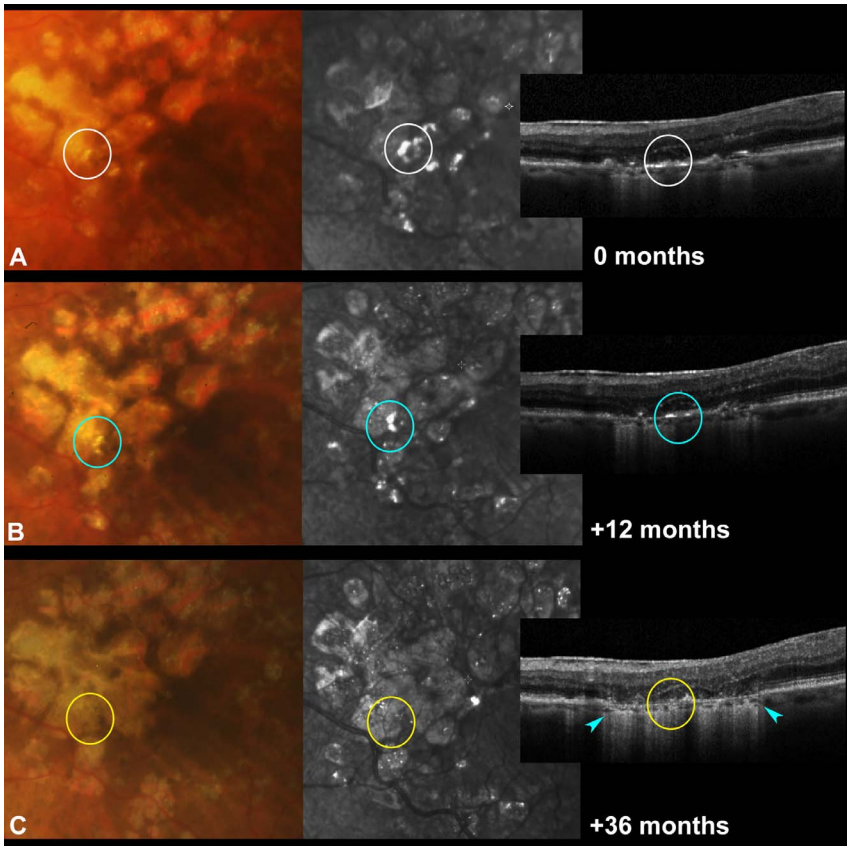

FIGURE 4. Multimodal imaging of HCD dynamism in nonneovascular age-related macular degeneration. *Left*: Color fundus photography. *Middle*: NIR. *Right*: SD-OCT. This 78-year-old woman has large drusen and variable degrees of RPE and outer retinal atrophy in the left eye. cRORA was best appreciated by SD-OCT with hypertransmission of OCT signal into the choroid (*light blue arrowheads*). (**A**) HCDs visible at first follow-up (*white circle*) were located at the edge of the hypertransmission area with marked attenuation of overlying RPE with either its native basal lamina or basal laminar deposit (RPE-BL). (**B**) In the second sequence, HCDs associated with refractile drusen show fragmentation (*light blue circle*) and then complete resorption (*yellow circle*). (**C**) Increasing hypertransmission due to complete loss of the RPE-BL at 36 months after baseline.

signature,[9,13,14] although extensively calcified BrM, as in pseudoxanthoma elasticum, is reflective.[41,42] Noteworthy, in our series, isolated linear or multilinear hyperreflective bands lying on BrM, described as HCDs and representing cholesterol crystals, were associated with refractile drusen in 33.3% of cases. Although the high resolution of modern OCT devices enables accurate matching to corresponding histologic findings, further evidence is needed to validate OCT features that may occur simultaneously during the drusen lifecycle.

Our data on HCDs should be contextualized with knowledge of the physical forms of cholesterol present at different stages of AMD, which is in turn informed by decades of research on cardiovascular disease.[43] Cholesterol, an essential lipid with four 6-carbon rings, appears in two chemical forms (esterified [EC] and unesterified [UC]) and three physical forms (oily droplets, liposomes, and crystals) that differ by their relative content of EC, UC, and phospholipid.[44] Cholesterol crystals are 100% UC, and they leave a readily detectable tissue symbol, because common extractive solvents in histologic processing remove cholesterol crystals and leave an empty cleft in the tissue. Cholesterol crystals are hallmarks of mature atherosclerotic plaques, where they are found in both extracellular (lipid-rich plaque core) and intracellular (foam cells, i.e., macrophages) locations.[45–48] We previously have demonstrated that choroidal stroma and macrophages of hypercholesterolemic rabbits have cholesterol crystals visible by polarizing microscopy in unprocessed specimens and cholesterol clefts in histologically processed specimens.[16] Cholesterol crystals within vulnerable atherosclerotic plaque are visible with intravascular OCT as thin linear regions of high intensity[47,49] and have been validated by histology.[50,51] Intravascular OCT also reveals calcification as signal-poor regions, in contrast to the reflective crystals.[47,49]

Histologic studies of early AMD have concluded that a major difference between AMD and cardiovascular disease, which both involve lipoprotein-instigated disease in a subendothelial space, is the absence of cholesterol crystals from BrM and drusen. All drusen in the sub-RPE–BL space contain EC and UC.[52,53] The main component of soft drusen is loosely packed UC-rich whorls with EC lakes, together considered "membranous debris" by Sarks et al.[12,54] This material was later termed "lipoprotein-derived debris"[55] owing to multiple lines of evidence that it is derived from large apoB, E-lipoproteins secreted by the RPE, in a constitutive program of outer retinal lipid cycling.[55,56] In contrast, histologic studies of late AMD eyes demonstrate cholesterol crystals in avascular fibrosis, serous PED, hemorrhagic PED, and fibrovascular scar, which the current clinical imaging data support. The hypothesized unifying feature in these conditions is the replacement of lipid-rich soft druse contents with either fluid or a fibrotic material that is sufficiently hydrated to allow UC supersaturation and precipitation.[22,40] In our case series, the duration of HCDs was correlated with macular complication subtypes, and particularly the presence of MNV exhibited the longest persistence of

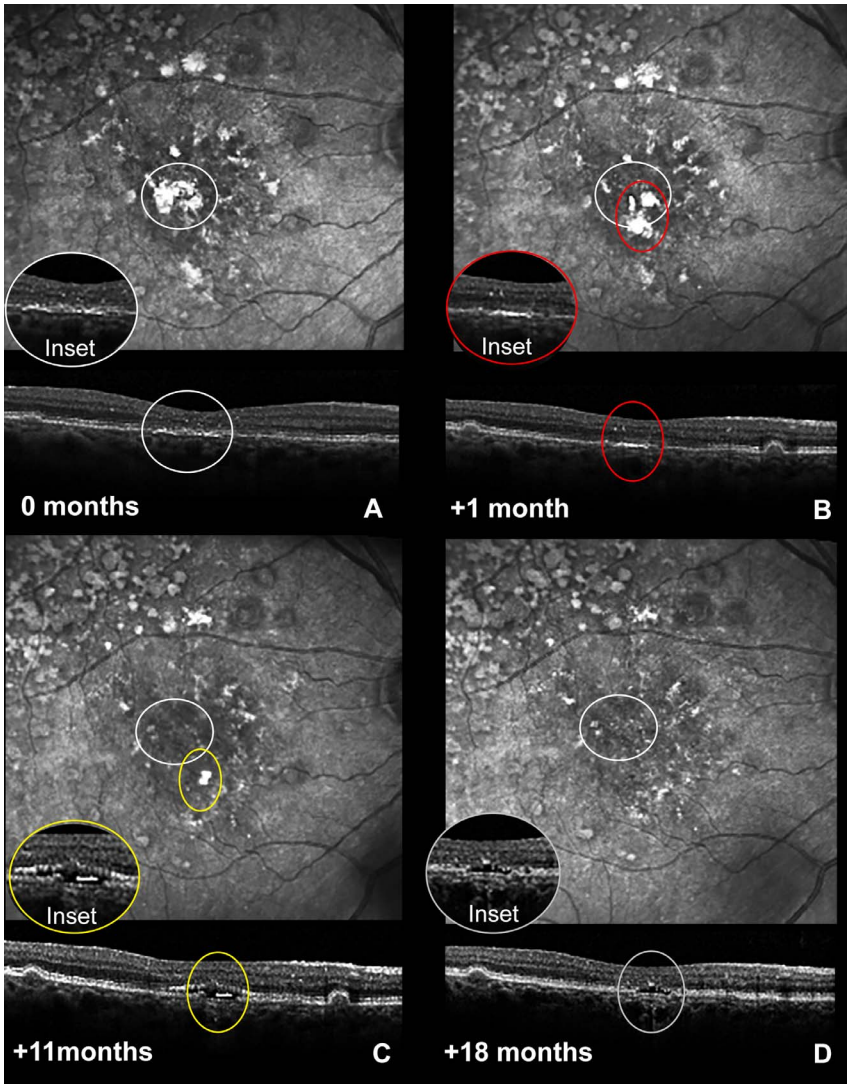

FIGURE 5. Movement and clearance of HCDs associated with retinal pigment epithelium aperture. Serial tracked NIR and SD-OCT B-scans of the right eye of a 77-year-old female. (**A**) At baseline, single linear hyperreflective HCDs in the fovea on NIR are seen to be clustered in the corresponding OCT B-scans (*white circle*). (**B**) One month later, the HCDs are located inferiorly (*red circle*) from their origin (*white circle*). (**C**) Eleven months after baseline, HCDs show partial resorption with further inferior movement (*yellow circle*). New subretinal fluid overlies a disruption in the retinal pigment epithelium. (**D**) HCDs were fully resorbed with residual subretinal fluid (*gray circle*). For further details see also Supplementary Video.

detectable HCDs. This finding suggests chronic exudation as a contributory mechanism for cholesterol crystal formation.[16]

We suggest that the appearance, movement, and dynamism of nonliving HCDs are readouts of the status of nearby living cells. It is possible that cholesterol crystals signify RPE degeneration, extrapolating from recent data on calcific nodules (hydroxyapatite) which is a soft drusen end-stage finding appearing as hyporeflective cores on OCT[28] and signifying a 4- to 6-fold increased risk for progression to advanced AMD. Because nodules appear concurrently with decreased fundus autofluorescence signal, this risk is attributed to a degeneration of overlying RPE that potentially raises extracellular pH and promotes nodule formation.[28] Further, cells in the sub-RPE–BL space along with the crystals include subducted RPE, multinucleated giant cells, presumed macrophages, and collagen-secreting fibroblasts, all of which could move, break up, or resorb crystals.[12,22,23,40,57] A similar range of cells associates with cholesterol crystals in Coats disease.[20,21] Cholesterol crystals, like calcific nodules, represent end-stages of lipid rich soft drusen, and dead drusen are not a good sign. It is true that soft drusen are a rich source of lipids that are modifiable to become proinflammatory and proangiogenic moieties that elicit local and systemic immune response.[56] However, RPE that is capable of maintaining a soft druse through physiologic secretions is probably also able to maintain photoreceptors. Recent cell culture experiments testing the effects of crystal exposure on nonconfluent RPE-derived cell lines have as yet uncertain relevance to our overall pathophysiology model which is based on longitudinal clinical imaging and histology.[58,59]

Strengths of this study were a longitudinal eye-tracked NIR/OCT follow-up of HCDs in nonneovascular AMD and an analysis identifying both specific multimodal imaging characteristics and HCD turnover as prognostic indicators of worse visual and anatomic outcomes. Limitations of this study included its retrospective nature, the lack of direct comparison

with a control group to assess a definite predictive model, and the use of commercial SD-OCT devices that did not provide raw linear reflectivity data useful for quantifying lesion reflectivity. Despite these limitations, we showed HCDs are a biomarker for the development of late-stage macular complications with clusters of HCDs in NIR adding further negative prognostic value for visual decline, and centrifugal movement associated with growth of cRORA. Further, extrapolating from the recognition of HIRD as an OCT biomarker for progression,[28,39,60] high reflectivity and dynamism of HCDs may be amenable to automated recognition and analysis to assess cellular activity in the sub-RPE–BL space. These new data will be useful in addressing the significance of HCDs in non-neovascular AMD that represent the end-stage of the drusen lifecycle preceding late-stage macular complications.

Acknowledgments

Supported by The Macula Foundation, Inc., New York, New York, United States, the Honors Center of Italian Universities (H2CU) (SF), Heidelberg Engineering, and Hoffman La Roche (CAC). The Department of Ophthalmology and Visual Science of the University of Alabama at Birmingham receives institutional support from EyeSight Foundation of Alabama and Research to Prevent Blindness, Inc.

Disclosure: **S. Fragiotta**, None; **P. Fernández-Avellaneda**, None; **M.P. Breazzano**, None; **C.A. Curcio**, None; **B.C.S. Leong**, None; **K. Kato**, None; **L.A. Yannuzzi**, None; **K.B. Freund**, Genentech (C), Optovue (C), Zeiss (C), Heidelberg Engineering (C), Allergan (C), Novartis (C)

References

1. Wong WL, Su X, Li X, et al. Global prevalence of age-related macular degeneration and disease burden projection for 2020 and 2040: a systematic review and meta-analysis. *Lancet Glob Health*. 2014;2:e106–e116.
2. Maguire MG, Martin DF, Ying GS, et al.; Comparison of Age-related Macular Degeneration Treatments Trials Research Group. Five-year outcomes with anti-vascular endothelial growth factor treatment of neovascular age-related macular degeneration: the comparison of age-related macular degeneration treatments trials. *Ophthalmology*. 2016;123:1751–1761.
3. Age-Related Eye Disease Study 2 Research Group. Lutein + zeaxanthin and omega-3 fatty acids for age-related macular degeneration: the Age-Related Eye Disease Study 2 (AREDS2) randomized clinical trial. *JAMA*. 2013;309:2005–2015.
4. Dolz-Marco R, Litts KM, Tan ACS, Freund KB, Curcio CA. The evolution of outer retinal tubulation, a neurodegeneration and gliosis prominent in macular diseases. *Ophthalmology*. 2017;124:1353–1367.
5. Curcio CA, Zanzottera EC, Ach T, Balaratnasingam C, Freund KB. Activated retinal pigment epithelium, an optical coherence tomography biomarker for progression in age-related macular degeneration. *Invest Ophthalmol Vis Sci*. 2017;58:BIO211–BIO226.
6. Tan ACS, Astroz P, Dansingani KK, et al. The evolution of the plateau, an optical coherence tomography signature seen in geographic atrophy. *Invest Ophthalmol Vis Sci*. 2017;58:2349–2358.
7. Tan ACS, Dansingani KK, Curcio CA, Freund KB. Author response: the evolution of the plateau, an optical coherence tomography signature seen in geographic atrophy. *Invest Ophthalmol Vis Sci*. 2017;58:6196.
8. Sadda SR, Guymer R, Holz FG, et al. Consensus definition for atrophy associated with age-related macular degeneration on OCT: classification of atrophy report 3. *Ophthalmology*. 2018;125:537–548.
9. Fleckenstein M, Charbel Issa P, Helb HM, et al. High-resolution spectral domain-OCT imaging in geographic atrophy associated with age-related macular degeneration. *Invest Ophthalmol Vis Sci*. 2008;49:4137–4144.
10. Staurenghi G, Sadda S, Chakravarthy U, Spaide RF; International Nomenclature for Optical Coherence Tomography Panel. Proposed lexicon for anatomic landmarks in normal posterior segment spectral-domain optical coherence tomography: the IN*OCT consensus. *Ophthalmology*. 2014;121:1572–1578.
11. Green WR, Key SN III. Senile macular degeneration: a histopathologic study. *Trans Am Ophthalmol Soc*. 1977;75:180–254.
12. Sarks JP, Sarks SH, Killingsworth MC. Evolution of geographic atrophy of the retinal pigment epithelium. *Eye (Lond)*. 1988;2(pt 5):552–577.
13. Moussa K, Lee JY, Stinnett SS, Jaffe GJ. Spectral domain optical coherence tomography-determined morphologic predictors of age-related macular degeneration-associated geographic atrophy progression. *Retina*. 2013;33:1590–1599.
14. Querques G, Georges A, Ben Moussa N, Sterkers M, Souied EH. Appearance of regressing drusen on optical coherence tomography in age-related macular degeneration. *Ophthalmology*. 2014;121:173–179.
15. Heiferman MJ, Fawzi AA. Discordance between blue-light autofluorescence and near-infrared autofluorescence in age-related macular degeneration. *Retina*. 2016;36(suppl 1):S137–S146.
16. Pang CE, Messinger JD, Zanzottera EC, Freund KB, Curcio CA. The onion sign in neovascular age-related macular degeneration represents cholesterol crystals. *Ophthalmology*. 2015;122:2316–2326.
17. Mukkamala SK, Costa RA, Fung A, Sarraf D, Gallego-Pinazo R, Freund KB. Optical coherence tomographic imaging of subretinal pigment epithelium lipid. *Arch Ophthalmol*. 2012;130:1547–1553.
18. Christakopoulos C, Pryds A, Larsen M. Subretinal lamellar bodies in polypoidal choroidal vasculopathy. *Acta Ophthalmol*. 2013;91:e248–e249.
19. Haik BG. Advanced Coats' disease. *Trans Am Ophthalmol Soc*. 1991;89:371–476.
20. Manschot WA, de Bruijn WC. Coats's disease: definition and pathogenesis. *Br J Ophthalmol*. 1967;51:145–157.
21. Ong SS, Cummings TJ, Vajzovic L, Mruthyunjaya P, Toth CA. Comparison of optical coherence tomography with fundus photographs, fluorescein angiography, and histopathologic analysis in assessing Coats disease [published online ahead of print November 21, 2018]. *JAMA Ophthalmol.* https://doi.org/10.1001/jamaophthalmol.2018.5654.
22. Li M, Dolz-Marco R, Messinger JD, et al. Clinicopathologic correlation of aneurysmal type 1 neovascularization in age-related macular degeneration. *Ophthalmol Retina*. 2019;3:99–111.
23. Li M, Dolz-Marco R, Huisingh C, et al. Clinicopathologic correlation of geographic atrophy secondary to age-related macular degeneration. *Retina*. 2019;39:802–816.
24. Balaratnasingam C, Yannuzzi LA, Curcio CA, et al. Associations between retinal pigment epithelium and drusen volume changes during the lifecycle of large drusenoid pigment epithelial detachments. *Invest Ophthalmol Vis Sci*. 2016;57:5479–5489.
25. Age-Related Eye Disease Study Research Group. The Age-Related Eye Disease Study system for classifying age-related macular degeneration from stereoscopic color fundus photographs: the Age-Related Eye Disease Study Report Number 6 *Am J Ophthalmol*. 2001;132:668–681.

Investigative Ophthalmology & Visual Science

26. Suzuki M, Curcio CA, Mullins RF, Spaide RF. Refractile drusen: clinical imaging and candidate histology. *Retina*. 2015;35: 859–865.
27. Oishi A, Thiele S, Nadal J, et al. Prevalence, natural course, and prognostic role of refractile drusen in age-related macular degeneration. *Invest Ophthalmol Vis Sci*. 2017;58:2198–2206.
28. Tan ACS, Pilgrim MG, Fearn S, et al. Calcified nodules in retinal drusen are associated with disease progression in age-related macular degeneration. *Sci Transl Med*. 2018; 10: eaat4544.
29. Cukras C, Agron E, Klein ML, et al. Natural history of drusenoid pigment epithelial detachment in age-related macular degeneration: Age-Related Eye Disease Study Report No. 28. *Ophthalmology*. 2010;117:489–499.
30. Mrejen S, Sarraf D, Mukkamala SK, Freund KB. Multimodal imaging of pigment epithelial detachment: a guide to evaluation. *Retina*. 2013;33:1735–1762.
31. Dolz-Marco R, Balaratnasingam C, Messinger JD, et al. The border of macular atrophy in age-related macular degeneration: a clinicopathologic correlation. *Am J Ophthalmol*. 2018; 193:166–177.
32. Sayegh RG, Sacu S, Dunavolgyi R, et al. Geographic atrophy and foveal-sparing changes related to visual acuity in patients with dry age-related macular degeneration over time. *Am J Ophthalmol*. 2017;179:118–128.
33. Hassenstein A, Meyer CH. Clinical use and research applications of Heidelberg retinal angiography and spectral-domain optical coherence tomography—a review. *Clin Exp Ophthalmol*. 2009;37:130–143.
34. Spaide RF. Fundus autofluorescence and age-related macular degeneration. *Ophthalmology*. 2003;110:392–399.
35. Schindelin J, Arganda-Carreras I, Frise E, et al. Fiji: an open-source platform for biological-image analysis. *Nat Methods*. 2012;9:676–682.
36. Holladay JT. Visual acuity measurements. *J Cataract Refract Surg*. 2004;30:287–290.
37. Ford ES, Li C, Pearson WS, Zhao G, Mokdad AH. Trends in hypercholesterolemia, treatment and control among United States adults. *Int J Cardiol*. 2010;140:226–235.
38. Querques G, Capuano V, Costanzo E, et al. Retinal pigment epithelium aperture: a previously unreported finding in the evolution of avascular pigment epithelium detachment. *Retina*. 2016;36(suppl 1):S65–S72.
39. Ouyang Y, Heussen FM, Hariri A, Keane PA, Sadda SR. Optical coherence tomography-based observation of the natural history of drusenoid lesion in eyes with dry age-related macular degeneration. *Ophthalmology*. 2013;120:2656–2665.
40. Li M, Huisingh C, Messinger J, et al. Histology of geographic atrophy secondary to age-related macular degeneration: a multilayer approach. *Retina*. 2018;38:1937–1953.
41. Gliem M, Fimmers R, Muller PL, et al. Choroidal changes associated with Bruch membrane pathology in pseudoxanthoma elasticum. *Am J Ophthalmol*. 2014;158:198–207.
42. Jensen OA. Bruch's membrane in pseudoxanthoma elasticum: histochemical, ultrastructural, and x-ray microanalytical study of the membrane and angioid streak areas. *Albrecht Von Graefes Arch Klin Exp Ophthalmol*. 1977;203:311–320.
43. Small DM. George Lyman Duff memorial lecture: progression and regression of atherosclerotic lesions: insights from lipid physical biochemistry. *Arteriosclerosis*. 1988;8:103–129.
44. Curcio CA, Presley JB, Millican CL, Medeiros NE. Basal deposits and drusen in eyes with age-related maculopathy: evidence for solid lipid particles. *Exp Eye Res*. 2005;80:761–775.
45. Baumer Y, McCurdy S, Weatherby TM, et al. Hyperlipidemia-induced cholesterol crystal production by endothelial cells promotes atherogenesis. *Nat Commun*. 2017;8:1129.
46. Bertazzo S, Gentleman E, Cloyd KL, Chester AH, Yacoub MH, Stevens MM. Nano-analytical electron microscopy reveals fundamental insights into human cardiovascular tissue calcification. *Nat Mater*. 2013;12:576–583.
47. Nishimura S, Ehara S, Hasegawa T, Matsumoto K, Yoshikawa J, Shimada K. Cholesterol crystal as a new feature of coronary vulnerable plaques: an optical coherence tomography study. *J Cardiol*. 2017;69:253–259.
48. Kellner-Weibel G, Yancey PG, Jerome WG, et al. Crystallization of free cholesterol in model macrophage foam cells. *Arterioscler Thromb Vasc Biol*. 1999;19:1891–1898.
49. Tearney GJ, Regar E, Akasaka T, et al. Consensus standards for acquisition, measurement, and reporting of intravascular optical coherence tomography studies: a report from the International Working Group for Intravascular Optical Coherence Tomography Standardization and Validation. *J Am Coll Cardiol*. 2012;59:1058–1072.
50. Liu L, Gardecki JA, Nadkarni SK, et al. Imaging the subcellular structure of human coronary atherosclerosis using micro-optical coherence tomography. *Nat Med*. 2011;17:1010–1014.
51. Tearney GJ, Jang IK, Bouma BE. Optical coherence tomography for imaging the vulnerable plaque. *J Biomed Opt*. 2006; 11:021002.
52. Curcio CA, Millican CL, Bailey T, Kruth HS. Accumulation of cholesterol with age in human Bruch's membrane. *Invest Ophthalmol Vis Sci*. 2001;42:265–274.
53. Malek G, Li CM, Guidry C, Medeiros NE, Curcio CA. Apolipoprotein B in cholesterol-containing drusen and basal deposits of human eyes with age-related maculopathy. *Am J Pathol*. 2003;162:413–425.
54. Sarks JP, Sarks SH, Killingsworth MC. Evolution of soft drusen in age-related macular degeneration. *Eye (Lond)*. 1994;8(pt 3):269–283.
55. Curcio CA, Johnson M, Huang JD, Rudolf M. Aging, age-related macular degeneration, and the response-to-retention of apolipoprotein B-containing lipoproteins. *Prog Retin Eye Res*. 2009;28:393–422.
56. Curcio CA. Soft drusen in age-related macular degeneration: biology and targeting via the oil spill strategies. *Invest Ophthalmol Vis Sci*. 2018;59:AMD160–AMD181.
57. Zanzottera EC, Messinger JD, Ach T, Smith RT, Curcio CA. Subducted and melanotic cells in advanced age-related macular degeneration are derived from retinal pigment epithelium. *Invest Ophthalmol Vis Sci*. 2015;56:3269–3278.
58. Hu Y, Lin H, Dib B, et al. Cholesterol crystals induce inflammatory cytokines expression in a human retinal pigment epithelium cell line by activating the NF-kappaB pathway. *Discov Med*. 2014;18:7–14.
59. Tian B, Al-Moujahed A, Bouzika P, et al. Atorvastatin promotes phagocytosis and attenuates pro-inflammatory response in human retinal pigment epithelial cells. *Sci Rep*. 2017;7:2329.
60. Lei J, Balasubramanian S, Abdelfattah NS, Nittala MG, Sadda SR. Proposal of a simple optical coherence tomography-based scoring system for progression of age-related macular degeneration. *Graefes Arch Clin Exp Ophthalmol*. 2017; 255:1551–1558.

Investigative Ophthalmology & Visual Science